Biosensors and Bioelectronics 126 (2019) 543–550

Contents lists available at ScienceDirect

Biosensors and Bioelectronics

journal homepage: www.elsevier.com/locate/bios

An ultrasensitive electrochemical immunosensor for procalcitonin detection based on the gold nanoparticles-enhanced tyramide signal amplification strategy

Pei Liu[a], Chao Li[b], Ruixuan Zhang[a], Qing Tang[a], Jia Wei[c], Yan Lu[a], Pingping Shen[a,*]

[a] State Key Laboratory of Pharmaceutical Biotechnology and The Comprehensive Cancer Center, Nanjing Drum Tower Hospital, MOE Key Laboratory of Model Animal for Disease Study, School of Life Sciences, Nanjing University, Nanjing 210046, PR China
[b] State Key Laboratory of Pharmaceutical Biotechnology and Collaborative Innovation Center of Chemistry for Life Sciences, School of Life Sciences, Nanjing University, Nanjing 210046, PR China
[c] The Comprehensive Cancer Center, Nanjing Drum Tower Hospital, The Affiliated Hospital of Nanjing University Medical School, Nanjing 210008, PR China

ARTICLE INFO

Keywords:
Antibiotic resistance
Procalcitonin
Immunosensor
AuNPs
Tyramide signal amplification

ABSTRACT

In this study, we established an ultrasensitive electrochemical immunosensor based on the gold nanoparticles-enhanced tyramide signal amplification (AuNPs-TSA) for the detection of procalcitonin (PCT, for discriminating bacterial infections from nonbacterial infections). Firstly, a facilely prepared, well-conducting reduced graphene oxide nanosheets/GNP (rGO-AuNPs) nanocomposite was synthesized and immobilized on the electrode surface to absorb more capture antibodies (Ab1). Next another nanocomposite, acting as a signal tool, was modified with detection antibody (Ab2) and horseradish peroxidase (HRP), and then backfilled by bovine serum albumin (BSA). Because a single AuNP is able to load multiple HRPs and BSAs, a number of tyramine labeled biotins (T-B) could be deposited on the proteins adhering to the surface of AuNPs. Moreover, the high affinity between streptavidin (SA) and biotins significantly increases the loading of streptavidin labeled horseradish peroxidase (SA-HRP). The amplification system which was based on the two nanocomposites mentioned above, effectively amplified the electric current signals. This immunosensor exhibits a wide dynamic detection range from 0.05 ng mL^{-1} to 100 ng mL^{-1} and with an ultralow detection limit of 0.1 pg mL^{-1}. We have successfully utilized this immunosensor to quantify the concentration of PCT in human serum samples, and the results suggest its potential use in clinical application.

1. Introduction

The misuse of antibiotics not only aggravates antibiotic resistance, but also causes severe side effects on human health (Buttmann and Rieckmann, 2010). Therefore, the accurate diagnosis of infection before employing the antibiotic therapy is important and clinically necessary. Procalcitonin (PCT), a sensitive biomarker of inflammation, is a FDA-approved marker of blood infection for guiding antibiotic therapy (Schuetz et al., 2018). In clinical settings, when PCT concentration in serum exceeds 0.5 ng mL^{-1}, the antibiotic therapy will be highly recommended (Tang et al., 2007). In addition, the serum PCT level also plays an advisory role in the diagnosis of sepsis, as higher than 2 ng mL^{-1} of PCT suggests the occurrence of sepsis (Schneider and Lam, 2007; Yu et al., 2016). Thus, the accurate detection of PCT in serum is crucial for effective early diagnosis and very helpful for further treatment guidance.

So far, numerous methods for detecting PCT based on immunoassay have been reported, including colorimetric immunoassay (Köszegi, 2002), chemiluminescence immunoassay (CMIA) (Morgenthaler et al., 2002), electrochemical immunoassay (Liu et al., 2014; Ribaut et al., 2016; Sipos and Urakawa, 2016), microfluidics immunoassays (Li et al., 2017), and fluorescence immunoassay (Chao et al., 2015). Due to the lack of signal amplification process in the detection system, these methods are either with low sensitivity or with narrow linear range. Hence, developing new methods for PCT detection are required.

Tyramide signal amplification (TSA) is a horseradish peroxidase (HRP) mediated signal amplification method. With the presence of hydrogen peroxide (H_2O_2), HRP is able to catalyze the phenolic part of tyramine to produce a radical-containing quinone-like structure on the C2 group. This “activated” tyramine then covalently binds to the tyrosine residues of nearby protein molecules (van Gijlswijk et al., 1997). Due to its good amplification effect and simple operations, TSA has

* Corresponding author.
E-mail address: ppshen@nju.edu.cn (P. Shen).

https://doi.org/10.1016/j.bios.2018.10.048
Received 18 July 2018; Received in revised form 25 September 2018; Accepted 20 October 2018
Available online 28 October 2018
0956-5663/

been widely used in ELISA (Park et al., 2012a, 2012b), immunohistochemistry (Wang et al., 2011), and in situ hybridization (Zubáčová et al., 2011) for the detection of protein (Akama et al., 2016), cell (Watakabe et al., 2010), and virus (Trang et al., 2015).

Herein, an ultrasensitive electrochemical immunosensor based on the gold nanoparticles-enhanced tyramide signal amplification (AuNPs-TSA) for detection of PCT has been developed. In this work, reduced graphene oxide nanosheets/GNP (rGO-AuNPs) nanocomposite was used to modify the working electrode sensing platform, to enlarge the amount of the immobilized capture antibodies (Ab1) (Chen et al., 2014). Another synthesized nanocomposite was employed as the carrier for HRP and detection antibody (Ab2). AuNPs have been reported to exhibit great chemical stability, large specific surface area, strong adsorption ability, good electrical conductivity, biocompatibility, and suitability (Chen et al., 2014; Hammond et al., 2016; Zhang et al., 2016). The use of AuNPs here could absorb more Ab2s and HRPs and meanwhile not affect the bioactivity of HRPs and Ab2s. In addition to the abovementioned advantages, HRP catalysis could also lead to the deposition of tyramine labeled biotins (T-Bs) to blocked bovine serum albumin (BSA) and hence further amplify the signal. This is not widely utilized in traditional TSA-based methods (Wu et al., 2014). This proposed immunosensor exhibits a wide linear range and an ultralow detection of limit for PCT. Most important, our results indicate that this immunosensor has good performance in human serum sample analysis, exhibiting its potential use in clinical diagnosis.

2. Experimental

2.1. Reagents and materials

Horseradish peroxidase (HRP), tyramide, and 1-ethyl-3-(3-dimethylaminopropyl)-carbodiimide hydrochloride (EDC), C-reactive protein (CRP), tumor necrosis factor-alpha (TNFα), and interleukin-6 (IL6) were purchased from Sigma-Aldrich (St. Louis, MO, USA). Azide-*n*-hydroxysuccinimide ester (N_3-NHS), dibenzocyclooctyl-polyethylene glycol-Thiol (DBCO-PEG-SH) were obtained from Nanocs Inc. (New York, USA). EZTM-Link Sulfo-NHS-Biotinylation was obtained from Thermo Fisher scientific (United Kingdom, USA). PCT, anti-PCT were made in our laboratory. Reduced graphene oxide nanosheets (rGO) were obtained from XFNANO, Inc. (Nanjing, China). 3, 3′, 5, 5′-tetramethylbenzidine (TMB) was purchased from Neogene (Lexington, KY) in the format of a ready-to-use reagent (enhanced K-blue substrate, H_2O_2 included). The synthesis of AuNPs was according to our previous report (Chao et al., 2015). Bovine albumin (BSA, standard grade) was commercially obtained from Alfa aesar (Tianjin, China). Clinical human serum samples were provided by Jingling Hospital (Nanjing, China). All other reagents were used as received.

2.2. Apparatus

Deionized water was purified through an Olst ultrapure K8 apparatus (Olst, Ltd., resistivity > 18 MΩ cm). Transmission electron microscopy (TEM) measurements were performed with a JEM-1200EX (120 kV) electron microscope (JEOL, Japan) under 120 kV accelerating voltage (H7650, Hitachi, Japan). Fourier Transform Infrared Spectroscopy (FTIR) analysis was performed on Nicolet IS10 (Thermo Fisher, USA). UV–vis diffuse reflectance spectrum measurements were performed with a Shimadzu UV-1800 spectrometer (Japan). Current-time curve (CT) measurements were conducted with a CHi660d electrochemical workstation (Shanghai Chenhua Instruments Co., LTD, China). The three-electrode system consisted of a modified glassy carbon electrode (GCE) as the working electrode, a platinum wire as the counter electrode, and an Ag/AgCl electrode saturated with KCl as the reference electrode.

2.3. Synthesis of AuNPs

AuNPs have gained an increasing interest due to their special features, easy surface functionalization, high stability and biological compatibility, and especially, due to their extraordinary optical and electrical properties (Liu et al., 2016; Madni et al., 2018). AuNPs were prepared by means of citrate reduction of $HAuCl_4$ according to the literature with certain modifications (Li et al., 2015). First of all, 100 mL of 0.01% (w/v) $HAuCl_4$ solution was prepared. Second, 3.5 mL of 1% (w/v) trisodium citrate was added to the above refluxing solution while stirring and boiling for 15 min. Finally, after continued stirring for another 30 min, the solution was cooled down to room temperature.

2.4. Synthesis of rGO-AuNPs

For preparation of rGO-AuNPs, briefly, 2 mL rGO dispersion (1 mg mL^{-1}) was mixed with 20 μL polylysine solution (2 mg mL^{-1}) and ultrasonication for 30 min at room temperature. Afterward, the excess reagents were removed by centrifuging at 12000 rpm for 5 min. After that, rGO-polylysine and AuNPs were mixed quickly. Finally, rGO-AuNPs were obtained by removing the non-integrated AuNPs away through centrifugation and washing with ultrapure water. After being washed and undergoing centrifugation several times, the collected samples were re-dispersed in 2 mL ultrapure water and stored at 4 °C before use.

2.5. Preparation of AuNPs-HRP-PEG-Ab2

AuNPs-HRP-PEG-Ab2 was prepared according to the following steps. AuNPs and HRP were mixed at a molar ratio of 1:5 (AuNPs to HRP) and stirred for 1 h at room temperature. Then reaction of Ab2 and N_3-NHS could proceed easily and quickly in the presence of EDC as cross-linking reagent within 1 h. Bioorthogonal chemistry (Pan et al., 2017) with high specificity and efficacy occurred easily between azide-modified Ab2 (Ab2-N_3) and DBCO-PEG-SH. Finally, the two solutions (AuNPs-HRP and Ab2-PEG-SH) were transferred to a clean centrifugal tube, stirred overnight at 4 °C temperature, and centrifuged at 12000 rpm for 15 min at 4 °C to remove excess Ab2-PEG-SH. The Ab2-PEG-SH modified on AuNPs through thiol groups (Lee et al., 2014). After washing 3 times using PBS (pH 7.4, 0.01 M), the AuNPs-HRP-PEG-Ab2 was diluted in PBS and stored at −20 °C.

2.6. Fabrication of rGO-AuNPs based electrode

A glassy carbon electrode (GCE, 3 mm in diameter) was carefully polished to a mirror-like surface with 0.3 μm alumina powders for 5 min and sonicated in ethanol and ultrapure water respectively. The rGO-AuNPs, prepared as described, were dropped onto the GCE surface and dried at room temperature. We could observe the AuNPs were well-distributed into rGO sheets, and this phenomenon could be attributed to the effect of the residual oxygen functional groups in rGO on immobilization of metal nanoparticles (Lee et al., 2014). While it has been known that most oxygen functionalities on the basal planes of rGO are removed through chemical reduction by hydrazine (Park et al., 2012a, 2012b), the carboxylic acid groups at edge sites could remain at certain reduction conditions, and react with other nucleophilic groups such as alcohol or amine (Lee et al., 2013). Furthermore, higher density and connected network of AuNPs along the graphene edge can also enhance the electrochemical activity of the rGO-AuNPs modified GCE electrode, because the high density of AuNPs can increase the interface area, and the connected network structure provides efficient conducting channels for the electron transfer of $[Fe(CN)_6]^{3-/4-}$. As rGO-AuNPs exhibited high uniformity and excellent conductivity, which could provide abundant bonding sites for immobilization of Ab1, it is also easy to sensitively transmit and amplify electrochemical signals with them, thus they could serve as an ideal electrode substrate of an immunosensor. Next, a

solution containing 100 ng mL^{-1} anti-PCT was dropped on the rGO-AuNPs modified area of GCE surface and then the modified electrode was stored at 4 °C for 12 h. BSA (2% w/v) was employed to block possible remaining active sites and avoid the non-specific adsorption. At each step, carefully washing was indispensable for removing excess materials, and the finished immunosensor was stored at 4 °C for use.

2.7. Electrochemical determination of PCT

Based on the sandwich-type electrochemical immunoassay, the immunosensor was first incubated with target antigens for 30 min at 37 °C, then incubated with AuNPs-HRP-PEG-Ab2 for 30 min at 37 °C, and thus formed probe-Ab2/Ag/Ab1 format. Subsequently, the mixture of T-B and H_2O_2 in pH 7.4 PBS buffer solution was dropped onto the modified GCE electrodes for 15 min at 37 °C and rinsed. Finally, SA-HRP solution was coated on the electrodes for 30 min at 37 °C. After being washed, the immunosensor acted as the working electrode and carried out the current (I)-versus-time (t) decay curve at 100 mV for different concentrations of PCT, which reaches a plateau within 100 s. The amperometric signal is logarithmically related to the PCT concentration.

3. Results and discussion

3.1. Principle of the proposed electrochemical immunosensor

In the present study, a gold nanoparticles-enhanced tyramide signal amplification (AuNPs-TSA) was fabricated for high sensitivity determination of PCT. This immunosensor took advantage of flexible combination of nanomaterials and TSA that resulted in remarkable achievement in the ultrasensitive quantification of target PCT. As shown in Scheme 1, the synthesized nanocomposite rGO-AuNPs were used as carriers for Ab1. The nanocomposite rGO-AuNPs modified on electrode is not only increased the binding sites due to high surface-area-to-volume ratios, but also enhanced the surface conductivity and π-π conjugation capability. Then the antigen PCT was captured by the specific antigen-antibody interaction. Another nanocomposite AuNPs-HRP-PEG-Ab2 conjugated to specific anti-PCT was utilized as a signal tool. In addition, this nanocomposite has two advantages compared with Ab2-HRP: depending on AuNPs excellent special features of easy surface functionalization, high stability and biological compatibility, much more Ab2s and HRPs could be participated in the binding reaction. Meanwhile, it could deposited considerably more biotin-tyramine on proteins coated on AuNPs. At last, it is believed that the presence of SA-HRP provided a greatly enhanced current signal in the following electrochemical biosensing. In this immunosensor, nanocomposites could amplify the signal and thus improve the sensitivity of PCT detection. These advantages make the immunosensor an ideal platform for detection of PCT with low concentrations (< 0.05 ng mL^{-1}).

3.2. Characterization of the nanocomposites

Highly efficient synthesis of the nanocomposites are crucial to the implementation of this immunosensor. To verify morphologies and sizes of rGO and rGO-AuNPs, we performed a detailed characterization of these nanocomposites using transmission electron microscopy (TEM) and UV–vis spectrophotometry. The TEM image clearly shows that AuNPs densely distributed on rGO with the diameter of approximately 21 ± 1.5 nm (Fig. 1B-E). It is well-established that the nanocomposites with numerous AuNPs can exhibit highly desirable binding sites due to their high surface-area-to-volume ratios (Navya and Daima, 2016). In addition, as shown in Fig. 1F, it is obvious that the rGO-AuNPs dispersion exhibits two characteristic peaks, one of which is at 231 nm corresponding to π→π* transitions of aromatic C=C bonds (Lu et al., 2011; Xie et al., 2017) and the other is at 521 nm attributing to the adsorption of the AuNPs (Ajdari et al., 2017). Therefore, these results demonstrate that the rGO-AuNPs nanocomposite were synthesized successfully, confirming the presence of AuNPs on the rGO surface, which could be considered as a nanocarrier to anchor large amounts of Ab1.

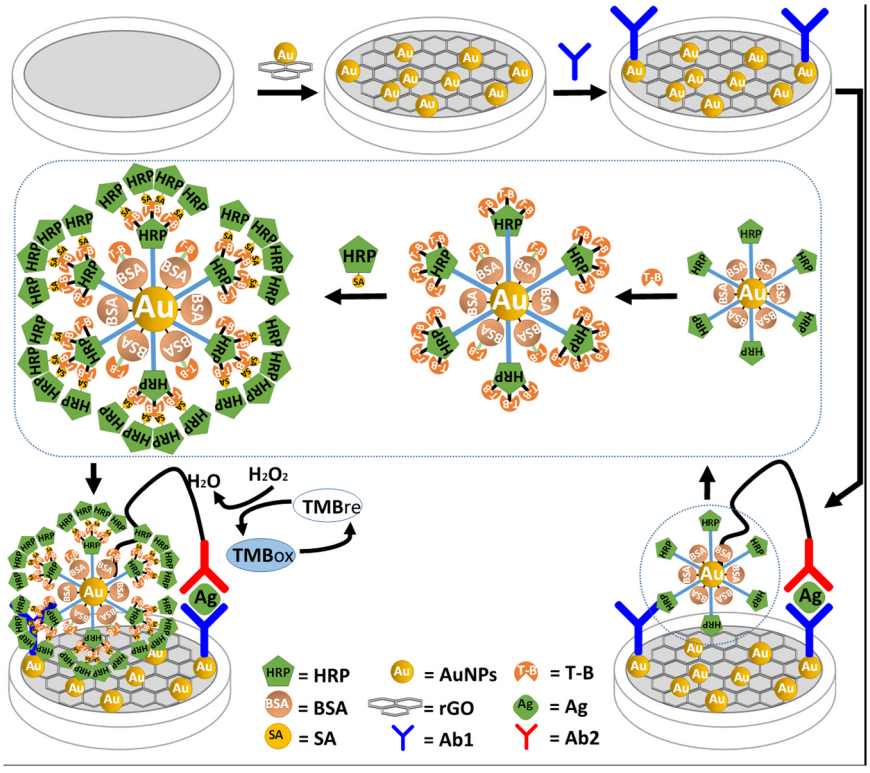

Scheme 1. Schematic procedure for the fabrication of the PCT immunosensor.

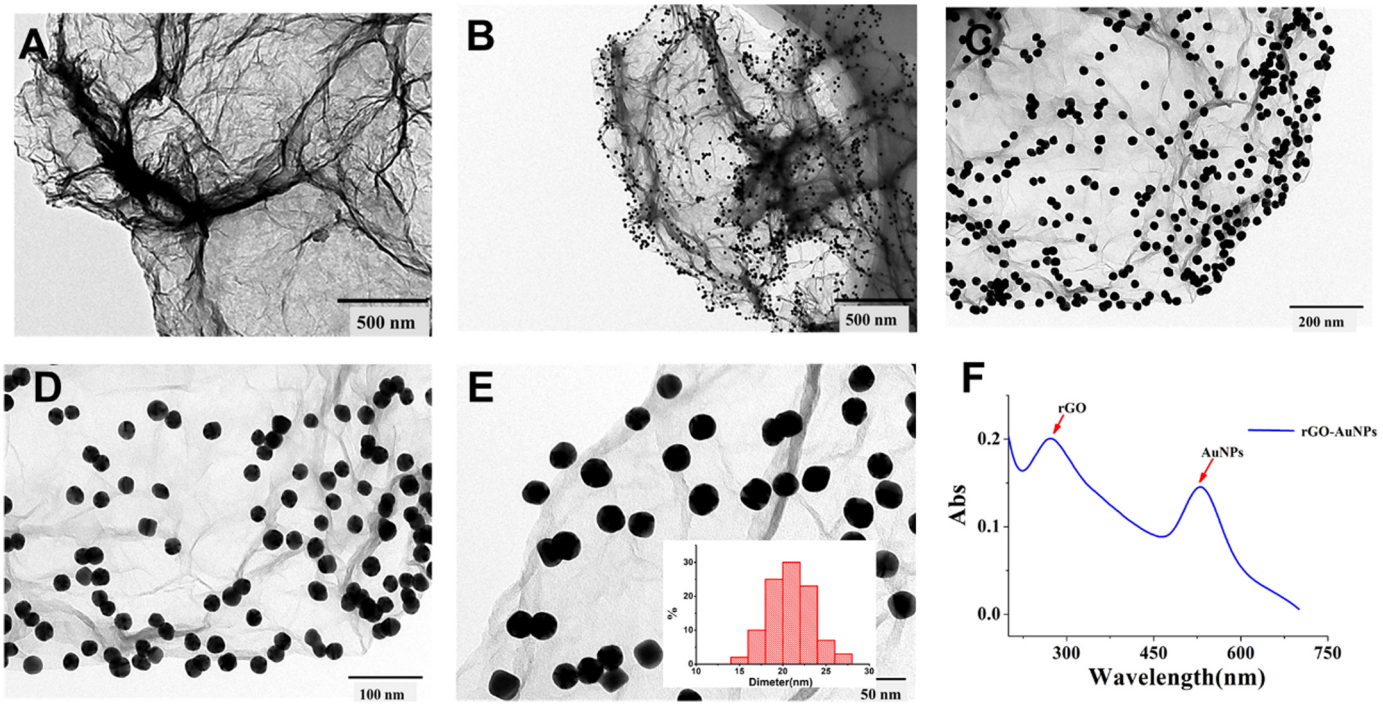

Fig. 1. TEM images of (A) reduced Graphene, (B-E) rGO-AuNPs, and (F) absorption spectra of solutions containing rGO-AuNPs.

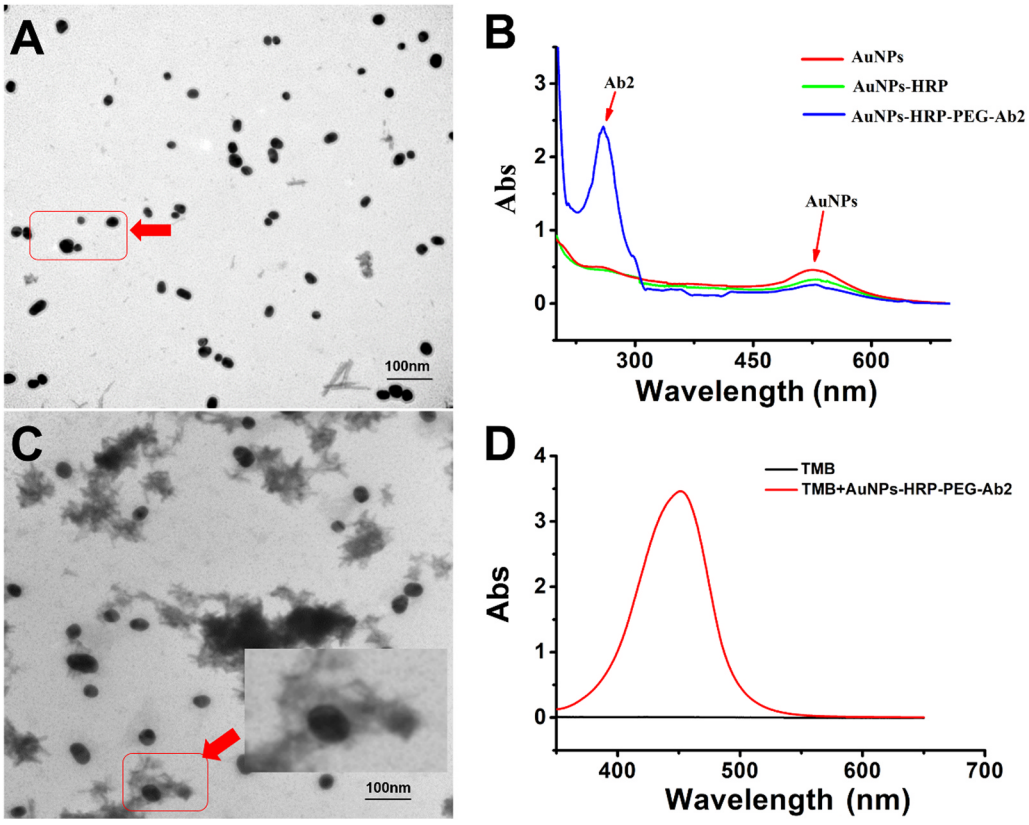

Fig. 2. (A)TEM image of AuNPs-HRP, (B)UV–vis spectra of AuNPs, AuNPs-HRP nanocomposite, and AuNPs-HRP-PEG-Ab2 nanocomposite (C) TEM image of AuNPs-HRP-PEG-Ab2 nanocomposite after incubation with tyramide-biotin and SA-HRP. (D) UV–vis spectra of TMB solution prior to the reaction with AuNPs-HRP-PEG-Ab2 and stopped by H_2SO_4.

Next, in order to characterize the AuNPs-HRP-PEG-Ab2 nanocomposite, we have applied the negative staining TEM measurements. After coating with HRP and Ab2-PEG-SH on the AuNPs, a shadow coating was observed surrounding the dark Au core (Fig. 2A). Fig. 2B shows the UV–vis absorption spectra of AuNPs, AuNPs-HRP and AuNPs-HRP-PEG-Ab2 nanocomposites. As expected, compared with bare AuNPs (curve red), a new absorption peak at 260 nm appears on the UV–vis absorption spectrum of AuNPs-HRP (curves green, blue), indicating that HRP and Ab2-PEG-SH were successfully bound onto AuNPs.

TEM image shows that a thick layer of protein was heaped all over the dark Au core after adding biotin-tyramine, H_2O_2 and SA-HRP (Fig. 2C). These results verified that AuNPs-HRP-PEG-Ab2 nanocomposite was successfully synthesized via layer by layer method. In the Fig. 2D, the UV–vis spectrum shown a satisfactory catalytic action of AuNPs-HRP-PEG-Ab2 in the presence of tetramethylbenzidine and H_2O_2. Further, Fourier-transform infrared spectroscopy spectrum was employed to characterize the composition of protein and PEG of AuNPs-HRP-PEG-Ab2 nanocomposite (Fig. S1). The 843 cm-1, 1280 cm-^{1}, and 947 cm^{-1} peaks, which are the contributions from the crystalline region in PEG, can be clearly observed (Ferreira et al., 2016). To analyze the peak from 1550 cm^{-1} to 1750 cm^{-1}, the convolution integral formula was also performed. The peaks between 1660 cm^{-1} and 1690 cm^{-1} can be assigned to the amide I modes of turn's structure (Bagchi et al., 2009). The band of the β-sheet vibration 1631 cm^{-1}, in our experiments is observed in Fig. S1(Nan et al., 2016; Zuckerman et al., 2015). We also used dynamic light scattering (DLS) technology to analyze the catalytic T-B deposition function of AuNPs-HRP-PEG-Ab2. In Fig. S2, the size of AuNPs-HRP-PEG-Ab2 nanocomposite ranges from 50 nm to 449 nm after being incubated with biotin-tyramine, H_2O_2, and SA-HRP, the final complexes show that there might be two or more layers formed according to the size.

3.3. Electrochemical characterization of the proposed immunosensor

As shown in Fig. 3A, the impedance change (charge-transfer resistance, R_{et}), which corresponds to the diameter of the semicircle in the Nyquist plot, is used to characterize the stepwise fabrication processes of the immunosensor. It is observed that the EIS of bare GCE (curve a) and rGO-AuNPs/GCE (curve b) display an almost straight line in the Nyquist plot. Subsequently, the R_{et} increased (curve c) when the electrode was modified with Ab1, which suggest that the Ab1 was successfully immobilized on the surface and formed an additional barrier blocking the electron exchange between the redox probe and the electrode. After BSA and PCT were gradually immobilized on the electrode surface, the R_{et} increased again (curve d, curve e), indicating that the formed immunocomplex blocked the electron transfer. In Fig. 3B, cyclic voltammograms (potential/E vs. current/I) shows the stepwise fabrication processes of the immunosensor. After incubating the immunosensor with Ab1, BSA, and PCT, the background currents decreased (curve b, d, and e), indicating the formation of antigen-antibody composite on the surface of the immunosensor hindered the current transmission.

3.4. Characterization of the signal amplification strategy

To verify the advantage of the developed immunoassay using AuNPs-HRP-PEG-Ab2 nanocomposite to connect TB and SA-HRP, a study was carried out to compare the electrochemical responses between an Ab2-HRP probe and our AuNPs-HRP-PEG-Ab2 probe. Fig. 4A shows that the presence of AuNPs-HRP-PEG-Ab2 not only greatly improved the deposition of T-B, and increased the adsorption of SA-SRP, but also significantly augmented the change of current. The underlying mechanism might be due to the fact that AuNPs possessed a high surface-to-volume ratio, which could enhance the immobilized amount of HRPs and Ab2s. To demonstrate the important role of TSA, we performed immunoassays with or without adding T-B. When T-B was absent, variation of current signal for PCT changes is small. In contrast, when T-B was present, the amplitude of variation of the current signal is much larger. These results indicate that the AuNPs-TSA strategy can greatly improve the performance of electrochemical immunosensor.

3.5. Optimization of immunoassay conditions

To achieve better analytical performance of the proposed immunosensors for PCT detection, we further optimized both the concentration of T-B and the amount of HRP coating on AuNPs. To guarantee enough T-B depositing on the nearby proteins, different concentrations of T-B (1–8 μM) were tested. When the concentration of T-B is lower than 7 μM, it exhibited a dose-dependent response, in that the signal increased correspondingly with T-B. However, the current signal reached a plateau when the T-B concentration is 7 μM (Fig. 4B). Thus, 5 μM T-B is used as the optimal concentration. Furthermore, in order to avoid the interference of free tyramide or biotin in subsequent experiments, High Performance Liquid Chromatography (HPLC) method has been utilized for the purification of T-B (Fig. S3). We have also optimized the amount of HRP coating on AuNPs and Fig. 4C reveals that the appropriate of HRP coating on AuNPs was 8 μM.

3.6. Analytical performance of immunosensor for PCT detection

Under the optimal experiment condition, the sensitivity and dynamic range of the immunosensor for PCT detection were examined by current-time technique. As anticipated, the electrochemical response

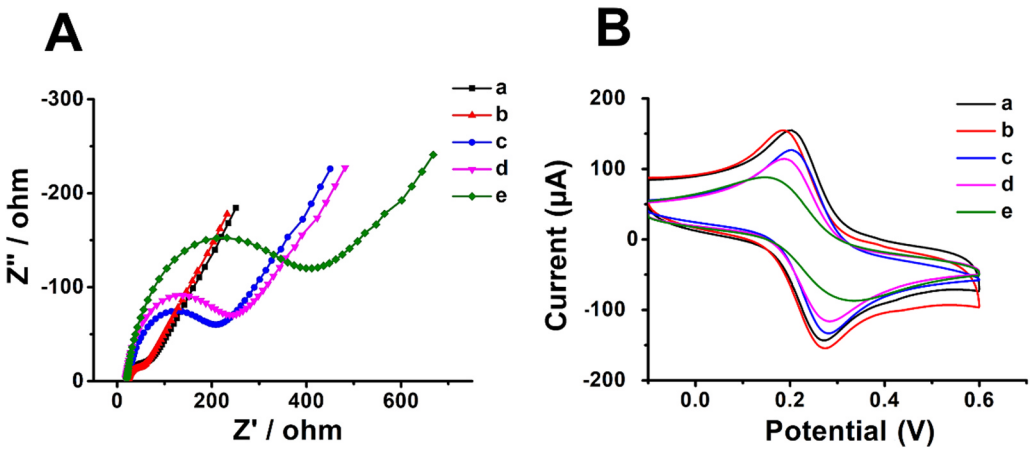

Fig. 3. (A) EIS of modified electrode in 0.1 M [Fe (CN) $_6]^{3-/4-}$ containing 0.1 M KCl after each assembling step of the immunosensor preparation procedure. (a) Bare GCE, (b) GCE/rGO-AuNPs, (c) GCE/BSA, (d) GCE/rGO-AuNPs/BSA/Ab1, (e) and GCE/rGO-AuNPs/BSA/Ab1/PCT in 1.0 M KCl solution containing 0.1 M $K_3[Fe(CN)_6]$ solution. (B) CVs of different electrodes. (a) Bare GCE, (b) rGO-AuNPs nanocomposite modified GCE, (c) BSA blocked GCE, (d) Ab1 immobilized rGO-AuNPs nanocomposites modified GCE, (e) Ab1 captured PCT immobilized rGO-AuNPs GCE in a 1.0 M KCl solution containing 0.2 M $K_3[Fe(CN)_6]$ solution.

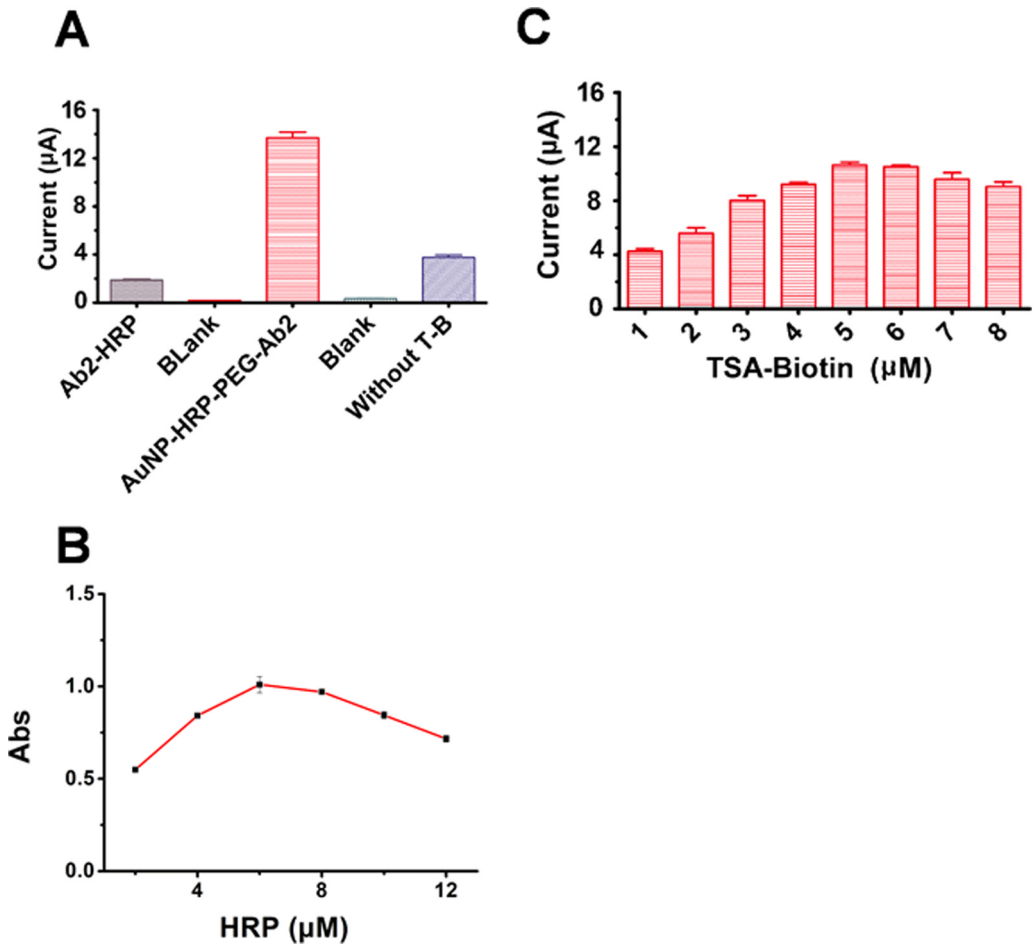

Fig. 4. (A) The current signal changed in the present of T-B is higher than that without T-B and non-enhanced methods. (B) Optimization of T-B concentration. (C) Optimization of HRP concentration.

increases along with the elevated concentration of PCT in the range of 0.05 ng mL^{-1} to 100 ng mL^{-1} (Fig. 5A). The calibration plot displays a good linear correlation between the current-time curve and the logarithm of PCT concentration (Fig. 5B). The limit of detection is calculated to be 0.1 pg mL^{-1} which is three times the standard deviation above the blank. Table S2 compared the present work's figures of merit to the recent reported values in the literature.

3.7. Specificity and stability of immunosensor

The specificity and stability of our immunosensor has also been verified by using several control species including C-reactive protein (CRP), tumor necrosis factor-alpha (TNFα), and interleukin-6 (IL6). As shown in Fig. 5C, the current response of CRP, TNFα, IL6 and even their mixture are nearly the same as the blank current. In sharp contrast, the current of PCT (0.5 ng mL^{-1}) dramatically increased. In addition, the mixture of the above proteins with PCT did not affect the signal of PCT at all, suggesting that the designed immunosensor is specific for PCT. Fig. 5D depicts the stability of immunosensor in the presence of 0.5 ng mL^{-1} PCT. The prepared electrodes are stored at 4 °C for two weeks. The current response only reduces 3.49% after 7 days' storage and 3.68% after 14 days respectively, suggesting that our immunosensor is pretty stable when stored at 4 °C.

3.8. Analysis of clinical serum samples

For the utilization of immunosensor, the applicability of analyzing human samples is of great importance. PCT were added into the normal human serum to obtain three different concentrations. The recovery values in the range of 98.8–104% are acceptable (Table S1), indicating that our immunosensor can potentially detect the PCT in serum samples. Furthermore, ten serum samples were measured in comparison with CMIA and each sample was measured at least three times. The relative errors between the two methods ranges from −9.25% to −3.35%, indicating that the electrochemical immunosensor has a good accuracy for clinical sample detection. We have compared the analytical performance of our AuNPs-TSA immunosensor with current methods used by commercial kits for PCT detection in terms of LOD, detection range, measurement time, and the sample consumption as listed in Table S2. Our immunosensor not only meets the clinical requirements, but also has advantages in small sample consumption.

4. Conclusion

In summary, we have developed an ultrasensitive electrochemical immunosensor based on the AuNPs enhanced TSA for detecting PCT. The rGO-AuNPs nanocomposite modified on electrode can not only

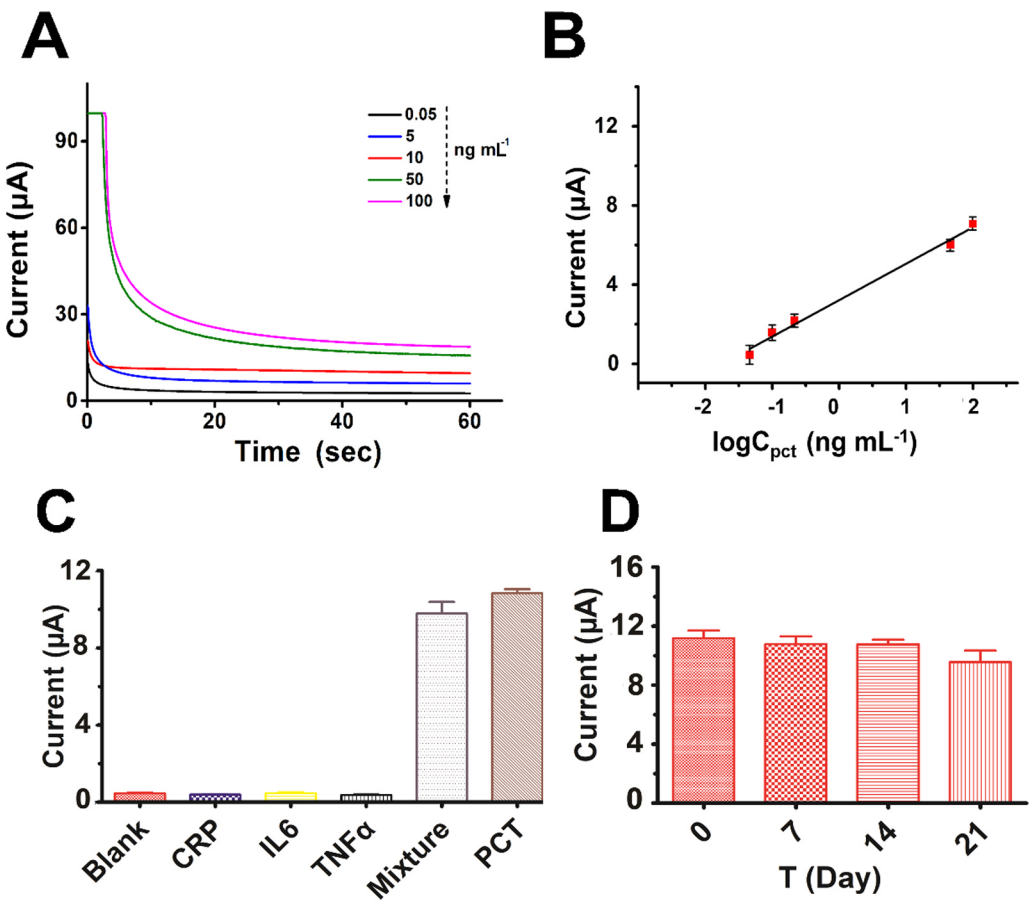

Fig. 5. (A) CT profiles of the immunosensor in exist of different concentrations of PCT in 0.01 M pH 7.6 PBS (containing 0.5% BSA). PCT concentration was 0.05–100 ng mL^{-1}. (B) The calibration curve of the immunosensor. (C) Specificity of the immunosensor. (D) The stability of the biosensor. Error bars represent standard deviations of three parallel experiments.

provide more attachment sites for the capture antibodies, but also increase the electrical conductivity of the electrodes. Moreover, a new AuNPs-HRP-PEG-Ab2 nanocomposite was synthesized to further enhance the output signal of this immunosensor. Thus, the present combination of nanomaterials and TSA successfully led to the construction of an ideal immunosensor and provided benefits including acceptable reproducibility, low LOD, wide linear range and remarkable sensitivity. Consequently, it is believed that this immunosensor could be promisingly used for clinical early diagnosis of bacterial infections and also for guiding antibiotic therapy due to its ability for highly sensitivity detection.

Acknowledgements

This research was financed by grants from the National Key Research and Development Plan (2017YFA0205400, 2017YFA0506000) and National Natural Science Foundation of China (81673439, 81473220). We thank Professor Scott Davis for critical comments and grammatical correction of the manuscript.

Appendix A. Supplementary material

Supplementary data associated with this article can be found in the online version at doi:10.1016/j.bios.2018.10.048.

References

Ajdari, N., Vyas, C., Bogan, S.L., Lwaleed, B.A., Cousins, B.G., 2017. Nanomedicine 13 (4).
Akama, K., Shirai, K., Suzuki, S., 2016. Anal. Chem. 88 (14), 7123.
Bagchi, S., Falvo, C., Mukamel, S., Hochstrasser, R.M., 2009. J. Phys. Chem. B 113 (32), 11260–11273.
Buttmann, M., Rieckmann, P., 2010. Expert Rev. Neurother. 10 (5), 791.
Chao, L., Yang, Y., Wei, L., Wang, X., Wang, Z., Yin, Y., Li, G., 2015. Theranostics 5 (1), 62–70.
Chen, G., Tong, H., Gao, T., Chen, Y., Li, G., 2014. Anal. Chim. Acta 849, 1–6.
Ferreira, D.P., Conceição, D.S., Calhelha, R.C., Sousa, T., Socoteanu, R., Ferreira, I.C., Vieira Ferreira, L.F., 2016. Carbohydr. Polym. 151, 160–171.
Hammond, J.L., Formisano, N., Estrela, P., Carrara, S., Tkac, J., 2016. Essays Biochem. 60 (1), 69–80.
Köszegi, T., 2002. J. Biochem. Biophys. Methods 53 (1), 157–164.
Lee, J.U., Lee, W., Jin, W.Y., Sang, S.Y., Sang, B.L., Jung, B.M., Kim, B.S., Byun, J.H., 2013. J. Mater. Chem. A 1 (41), 12893–12899.
Lee, J.U., Lee, W., Sang, S.Y., Kim, J., Byun, J.H., 2014. Appl. Surf. Sci. 315 (1), 73–80.
Li, C., Shi, L., Tao, Y., Mao, X., Xiang, Y., Li, G., 2017. Sci. Rep. 7 (1), 10017.
Li, C., Yang, Y., Wei, L., Wang, X., Wang, Z., Yin, Y., Li, G., 2015. Theranostics 5 (1), 62–70.
Liu, F., Xiang, G., Yuan, R., Chen, X., Luo, F., Jiang, D., Huang, S., Li, Y., Pu, X., 2014. Biosens. Bioelectron. 60 (22), 210–217.
Liu, Y.B., Yang, X., Simmons, G., 2016. Insects 7 (4), 71.
Lu, W., Ning, R., Qin, X., Zhang, Y., Chang, G., Liu, S., Luo, Y., Sun, X., 2011. J. Hazard. Mater. 197 (6), 320–326.
Madni, A., Noreen, S., Maqbool, I., Rehman, F., Batool, A., Kashif, P.M., Rehman, M., Tahir, N., Khan, M.I., 2018. J. Drug Target. 1.
Morgenthaler, N.G., Struck, J., Fischerschulz, C., Bergmann, A., 2002. Clin. Chem. 48 (5), 788–790.
Nan, Q., Zhang, S., Jiang, J., Corder, S.G., Qian, Z., Zhou, Z., Lee, W., Liu, K., Wang, X., Li, X., 2016. Nat. Commun. 7, 13079.
Navya, P.N., Daima, H.K., 2016. Nano Converg. 3 (1), 1.
Pan, H., Li, W.J., Yao, X.J., Wu, Y.Y., Liu, L.L., He, H.M., Zhang, R.L., Ma, Y.F., Cai, L.T., 2017. Small 13 (17), 1604036.
Park, S., Hu, Y., Hwang, J.O., Lee, E.S., Casabianca, L.B., Cai, W., Potts, J.R., Ha, H.W., Chen, S., Oh, J., 2012a. Nat. Commun. 3 (48), 638.
Park, S., Hu, Y., Jin, O.H., Lee, E.S., Casabianca, L.B., Cai, W., Potts, J.R., Ha, H.W., Chen, S., Oh, J., 2012b. Nat. Commun. 3 (48), 638.
Ribaut, C., Voisin, V., Malachovská, V., Dubois, V., Mégret, P., Wattiez, R., Caucheteur, C., 2016. Biosens. Bioelectron. 77, 315–322.
Schneider, H.G., Lam, Q.T., 2007. Pathology 39 (4), 383–390.
Schuetz, P., Wirz, Y., Sager, R., Christcrain, M., Stolz, D., Tamm, M., Bouadma, L., Luyt, C.E., Wolff, M., Chastre, J., 2018. Lancet Infect. Dis.
Sipos, A.J., Urakawa, H., 2016. Lett. Appl. Microbiol. 62 (2), 199–206.
Tang, B.M., Eslick, G.D., Craig, J.C., Mclean, A.S., 2007. Lancet Infect. Dis. 7 (3), 210–217.
Trang, N.T., Hirai, T., Ngan, P.H., Lan, N.T., Fuke, N., Toyama, K., Yamamoto, T., Yamaguchi, R., 2015. J. Vet. Diagn. Invest. 27 (3), 326–331.

van Gijlswijk, R.P., Zijlmans, H.J., Wiegant, J., Bobrow, M.N., Erickson, T.J., Adler, K.E., Tanke, H.J., Raap, A.K., 1997. J. Histochem. Cytochem. 45 (3), 375.
Wang, N., Gibbons, C.H., Freeman, R., 2011. J. Histochem. Cytochem. 59 (4), 382–390.
Watakabe, A., Komatsu, Y., Ohsawa, S., Yamamori, T., 2010. Methods 52 (4), 367–374.
Wu, Y., Xue, P., Hui, K.M., Kang, Y., 2014. Biosens. Bioelectron. 52 (4), 180–187.
Xie, W., Tang, L., Ying, M., Liu, J., Pan, H., Du, M., 2017. RSC Adv. 7.
Yu, Y., Li, X.X., Jiang, L.X., Du, M., Liu, Z.G., Cen, Z.R., Wang, H., Guo, Z.H., Chang, P., 2016. Infect. Dis. 48 (1), 63–69.
Zhang, Y., Mckelvie, I.D., Cattrall, R.W., Kolev, S.D., 2016. Talanta 152, 410–422.
Zubáčová, Z., Krylov, V., Tachezy, J., 2011. Mol. Biochem. Parasitol. 176 (2), 135–137.
Zuckerman, D.M., Boucher, L.E., Xie, K., Engelhardt, H., Bosch, J., Hoiczyk, E., 2015. PLoS One 10 (3), e0121074.